Dynamics of Structure Formation in Crystallizable Block Copolymers

Pratima Rangarajan and Richard A. Register*

Department of Chemical Engineering, Princeton University, Princeton, New Jersey 08544

Douglas H. Adamson and Lewis J. Fetters

Exxon Research and Engineering Company, Annandale, New Jersey 08801

Wim Bras

Netherlands Organisation for Scientific Research and SERC Daresbury Laboratory, Warrington, Cheshire WA4 4AD, United Kingdom

Steven Naylor and Anthony J. Ryan

Manchester Materials Science Centre, University of Manchester Institute of Science and Technology, Manchester M1 7HS, United Kingdom

Received November 2, 1994; Revised Manuscript Received December 6, 1994®

ABSTRACT: The dynamics of crystallization-driven microphase separation in semicrystalline block copolymers are investigated using diblocks of ethylene−(ethylene-*alt*-propylene) (E/EP) and ethylene−ethylethylene (E/EE). Simultaneous, time-resolved small-angle and wide-angle X-ray scattering (SAXS and WAXS) on heating and cooling are used to study the formation of the microphase-separated lamellar structure and the crystallization of the ethylene blocks, respectively. Sharp first- and higher-order SAXS peaks (as many as four reflections) evolve rapidly and simultaneously on cooling from the homogeneous melt, characteristic of a highly-ordered domain structure with relatively sharp interfaces. These semicrystalline diblocks thus form microdomains which appear strongly segregated, even though the small undercoolings used would put amorphous block copolymers in the weak segregation regime. Crystallization of the E blocks exactly tracks the development of the microdomain structure. During the initial rapid structure development, the SAXS peak positions are constant, suggesting that the ordered structures nucleate and simply grow to fill the sample, without any accompanying internal rearrangement. At longer times, a small decrease of the microdomain spacing is observed, attributed to the relaxation of a structure initially out of equilibrium.

I. Introduction

In the last 5 years several groups have studied the development of ordered structures in block copolymers using time-resolved small-angle X-ray scattering (SAXS) and rheology.[1−4] In the materials studied to date, the domains formed by each block are amorphous; the driving force for microphase separation is the incompatibility between the blocks, characterized by χN_t, where χ is the Flory interaction parameter and N_t is the total number of segments in the copolymer. When a critical value of χN_t is exceeded, either by increasing the molecular weight or changing the temperature to increase χ, the block copolymer will form domains rich in one block.[5−7] Since the microphase separation is driven by a desire of the blocks to minimize unlike contacts, the type of microdomain obtained is a function of the relative block lengths: from spheres of the minority component at very asymmetric compositions to an alternating lamellar morphology for symmetric block copolymers.[8,9]

Investigations of symmetric block copolymers have concluded that microphase separation proceeds via a nucleation and growth mechanism when the undercooling—the difference between the measurement and microphase separation transition temperatures—is small.[1−3] The evolution of microstructure has been successfully modeled by an Avrami-type equation traditionally used to describe nucleation and growth processes. Floudas *et al.*[1] find that the kinetics deviate from the Avrami model when the undercooling is large, where the microstructure formation should proceed by a mechanism resembling spinodal decomposition, with a growth in amplitude of density fluctuations occurring throughout the material simultaneously.[10,11]

In contrast to purely amorphous systems, semicrystalline block copolymers can microphase separate by a second mechanism: crystallization of one or more of the blocks. The phase diagram for such block copolymers crystallized from a single-phase melt is much simpler than the incompatibility-driven phase diagram: an alternating lamellar morphology is obtained at all block copolymer compositions,[12] as assumed in theoretical treatments.[13,14] Since the driving force for microphase separation is crystallization, the mechanism and kinetics of the ordering process should differ from the block incompatibility-driven systems which have been studied thus far. Although time-resolved SAXS has been used to study the crystallization of various semicrystalline homopolymers and their blends,[15−17] much less work of this nature has been done on microphase separation of crystallizable copolymers. Recently, combined SAXS and wide-angle X-ray scattering (WAXS) studies of polyurethanes with crystallizable hard segments have found that the SAXS invariant and the integrated WAXS intensity grow simultaneously when the materials crystallize from a single-phase melt, indicating that crystallization dominates the formation of microstructure.[18]

* To whom correspondence should be addressed.

® Abstract published in *Advance ACS Abstracts,* February 1, 1995.

0024-9297/95/2228-1422$09.00/0

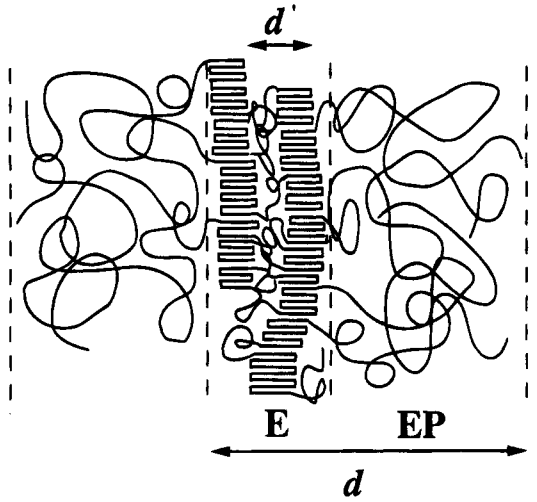

Figure 1. Schematic for the E/EP morphology d is the sum of the E and EP domain widths, and d' is the sum of the E crystalline and amorphous regions. Reproduced with permission from ref 12. Copyright 1993 American Chemical Society.

The present work investigates the mechanism of microphase separation in crystallizable block copolymers using diblocks of ethylene–(ethylene-*alt*-propylene), E/EP, as well as an ethylene–ethylethylene diblock, E/EE. Prior work on semicrystalline block copolymers has demonstrated that the final morphology is often path-dependent,[19,20] particularly when crystallization can occur from either a homogeneous or microphase-separated state. Based on our previous morphological work[12] and the χ relations determined by Bates *et al.*[21] for the E/EP and E/EE systems, all the diblocks studied here should crystallize from homogeneous melts. Figure 1 is a schematic representation of the E/EP diblock morphology found in our prior study.[12] Alternating lamellae of semicrystalline E and amorphous EP, of total domain width d, result in 2–3 relatively narrow SAXS peaks indicating a high degree of order.[12] The morphology within the E domain consists of crystallites of E alternating with amorphous E layers, with a repeat distance d'. This model has been proposed for crystallization occurring from single-phase melts; in studies of diblocks crystallizing from oriented two-phase melts, Cohen and co-workers[22] found that the E chain axis runs parallel to the domain interface, rather than perpendicular as shown in Figure 1. Whether the block copolymer melt is homogeneous or microphase-separated prior to crystallization may indeed strongly influence the kinetics and mechanism of crystallization.

Since the E block in our diblocks is actually a hydrogenated polybutadiene, it is essentially a random copolymer of ethylene with a minor amount of 1-butene. The crystallite thickness is governed by the frequency of butene units, which appear as ethyl branches along the chain.[23] Therefore block copolymers with E domains thick enough to accommodate multiple crystallites show a single broad SAXS peak due to d', similar to that shown by hydrogenated polybutadiene,[12] in addition to narrow peaks from the overall repeat distance d. Even though the broad d' peak indicates a distribution of intercrystallite distances, which should lead to some irregularity in the E domain thickness, the block copolymer SAXS patterns indicate a highly-ordered microdomain structure like that found in amorphous block copolymers. Interspersing these relatively irregular E domains with layers formed by the amorphous, near-monodisperse EP block evidently yields good long-range order. Therefore, although microphase separation is dependent on crystallization of the E chains, the development of the ordered structure should be modulated by the amorphous block. In this work combined synchrotron-based SAXS, WAXS, and differential scanning calorimetry (DSC) are employed to dynamically follow the crystallization-driven process of microphase separation in these materials, at both the unit cell and microdomain scales.

Table 1. Characterization Data

sample I.D. $M_{w(E)}/M_{w(am)}$	total M_w ($\times 10^3$)	f	peak T_m (°C)	initial w_c (WAXS)
E/EE 5/7	12.3[a]	0.41	106	0.49
E/EP 6/6	11.2	0.50	110	0.55
E/EP 6/8	13.9	0.40	111	0.54
E/EP 11/8	19.6	0.56	110	0.45
E/EP 7/15	21.7	0.30	106	0.50
E/EP 11/14	25.3	0.44	97	0.42
E/EP 19/30	48.8	0.38	110	0.56
E 52	52[a]	1	110	0.39

[a] From GPC only.

II. Experimental Section

A. Synthesis and Characterization. The E/EP precursors (high-1,4-butadiene–1,4-isoprene diblocks) and the E/EE precursor (1,4-butadiene–1,2-butadiene) were synthesized by sequential anionic polymerization in cyclohexane.[24] To create the high-1,2-butadiene precursor to the EE block, tetrahydrofuran was added at a concentration of 10 mol/mol of Li initiator after polymerization of the 1,4-butadiene block. Exhaustive hydrogenation of these precursors in heptane at 80–100 °C and 400 psi hydrogen using unpoisoned palladium on calcium carbonate or barium sulfate as catalyst results in the E/EP and E/EE diblocks.[12,25] A summary of the characterization information is presented in Table 1, where the diblocks are identified by the following sample code: sample type (E/EP or E/EE) followed by the molecular weights of the crystalline and amorphous blocks in kg/mol ($M_{w(E)}/M_{w(am)}$). The molecular weights were determined by low-angle laser light scattering (LALLS; Chromatix KMX-6) in cyclohexane whenever possible and by gel permeation chromatography (GPC) which also provides the polydispersity. Since the refractive index increments (dn/dc) of high-1,4-polyisoprene and polybutadiene are very similar in cyclohexane, a single dn/dc value of 0.105 cm^3/g was used in analyzing the data for the E/EP precursors.[12,26] High-temperature sequential GPC/LALLS (135 °C) was also performed on most of the E/EP diblocks and showed that no backbone changes occurred on hydrogenation.[12] ^{1}H nuclear magnetic resonance (NMR) on the precursors was used to determine the weight fraction of the E block (f, ±3% relative) and the microstructure of the precursor 1,4-isoprene (5–8% 3,4 units) and 1,4-butadiene (6–10% 1,2 units) blocks. Due to the unavailability of precursor for sample E/EP 11/14, high-temperature ^{13}C NMR was used, instead of ^{1}H NMR, on the hydrogenated diblock to analyze the microstructure. The percent 1,2 addition in the 1,4-butadiene block was used to calculate the frequency of ethyl branches in the E block. To characterize the precursor to the E/EE diblock, an aliquot of the first block was removed after polymerization, and its molecular weight (by GPC) and microstructure (by ^{1}H NMR) were determined. Comparison with GPC and ^{1}H NMR on the diblock yielded the overall composition and microstructure of the high 1,2 block (85% 1,2 units). This composition translates to 38 ethyl branches per 100 backbone carbons in the EE block after saturation. Fourier transform infrared (FTIR) spectroscopy was used to verify that there was no residual unsaturation in the samples. The peak melting temperatures of the samples were determined at 20 °C/minute, using a Perkin-Elmer DSC-7 calibrated with indium and mercury.

B. Time-Resolved Experiments. Time-resolved simultaneous SAXS/WAXS/DSC data were collected at beamline 8.2

Table 2. Isothermal Crystallization Results

sample I.D. $M_{w(E)}/M_{w(am)}$	$T_m - T_c$ (°C)	no. of SAXS peaks detected	final w_c (WAXS)	$t_{1/2}$ (s)	ΔQ (%)	$-\Delta d$ (%)
E/EE 5/7	8	3	0.16	138	10	0.6
E/EP 6/6	12	4	0.23	90	12	1.2
E/EP 6/8	12	4	0.33	68	14	2.6
E/EP 11/8	13	4	0.27	58	15	1.4
E/EP 7/15	8	4	0.27	132	12	0.8
E/EP 11/14	8	3	0.20	81	8	1.9
E/EP 19/30	12	3	0.35	153	7	0.9
E 52	11			≫720		
E 52	21	1[b]	0.20	<40[a]	2	0[b]

[a] Intensity growth begins ~30 s before t_0. [b] Denotes d' rather than d.

of the Synchrotron Radiation Source in Daresbury, England,[27] using a beam of $\lambda = 0.152$ nm X-rays measuring 3 × 0.3 mm² at the sample position. The SAXS patterns were collected with a Daresbury quadrant detector, calibrated with a wet rat tail tendon ($d = 67.0$ nm). The SAXS data presented here were subsequently smoothed with a 7-point triangle function and an additional 9-point triangle for $q > 0.5$ nm^{-1}. The WAXS data were acquired with a curved INEL detector which was cross-calibrated with WAXS data collected in reflection mode on a Phillips–Norelco wide-range goniometer using Cu Kα radiation.[12] Subsequent smoothing of the WAXS data employed a 5-point triangle function and an additional 11-point triangle for the data outside the crystallite peaks. The DSC unit is a modified Linkam THM microscope hot stage run by a high-resolution temperature controller.[28] A 1.0 × 2.5 mm² slot in the DSC cell holder and heating block allows the X-rays access to the sample. The sample cell consists of standard aluminum DSC pans (TA Instruments) with holes punched in both the pan and lid and covered with 0.025 mm thick mica windows. Scattering from the empty cell (including the DSC pan and windows) was subtracted from all SAXS and WAXS data. Polymer samples 1–2 mm thick were cut out of melt-cast films[12] which had been annealed at 70–85 °C. Controlled cooling is achieved via cold nitrogen vapor pumped through the heater block. The cell temperature was verified by comparison of crystallization half-times with those obtained from isothermal crystallization conducted on a Perkin-Elmer DSC-7. The temperature profile for the experiments was as follows: a 1 min hold at 30 °C, followed by a 20 °C/min ramp up to 148 °C, a 2 min hold at 148 °C, followed by a ~20 °C/min cool-down to the crystallization temperature (T_c) which was set for either 98 or 88 °C. Quench depths ($T_m - T_c$) for the samples are listed in Table 2. Data acquisition commenced after the 1 min hold at 30 °C; each SAXS or WAXS frame consists of the intensity integrated over a 6 s period.

III. Results

The molecular weights of the diblocks ranged from 12 000 to 49 000, with the weight fraction of the E block (f) ranging from 0.30 to 0.56. A hydrogenated high-1,4-polybutadiene labeled E 52 was also studied; all samples had polydispersities less than 1.07. All polymers except sample 11/14 have fewer than 18 ethyl branches/1000 backbone carbon atoms in the E block. Sample 11/14 has ~26 ethyl branches/1000 C, and this results in relatively poor microdomain ordering[12] and a low peak T_m (Table 1). The other samples, including the E 52, have T_m between 106 and 111 °C, indicating a similarity in the crystallite size and perfection.

Peak positions in the synchrotron SAXS data taken at 30 °C, before heating the samples, correspond very well to room temperature measurements made using a Kratky camera and desmeared.[12] The increased signal-to-noise ratio in the synchrotron data resulted in an increase (by 1) in the number of identifiable higher-order peaks for some samples. The higher-order peaks appear at integral multiples of the position of the first-order peak q^* (where $q = (4\pi/\lambda) \sin\theta$ is the scattering vector), indicating a well-ordered alternating lamellar morphology. Figure 2 shows the SAXS data for the isothermal crystallization of E/EP 11/8 at 98 °C plotted as the q^2-corrected[29] intensity q^2I versus q. The depth axis represents the time at T_c; the zero of the time axis (t_0) is set when the DSC controller first registers T_c. Some data sets prior to t_0 are shown in order to demonstrate that the featureless melt scattering persists for several seconds after t_0. Thus, in this data set no apparent morphological development has occurred before T_c is reached. As time progresses, all four peaks appear to grow at the same rate. The melting transition occurs similarly, with all four peaks fading in parallel. The concurrent development of all the orders is emphasized in the plot of SAXS peak intensity versus time in Figure 3, where the SAXS peak intensities have been determined by averaging over ±5 channels around the channel of maximum intensity.

Although the SAXS data provide information on growth of the microdomain morphology, they give little insight into the driving force for microphase separation: crystallization of the E chains. Figure 4 shows the WAXS frames for sample E/EP 11/8 corresponding

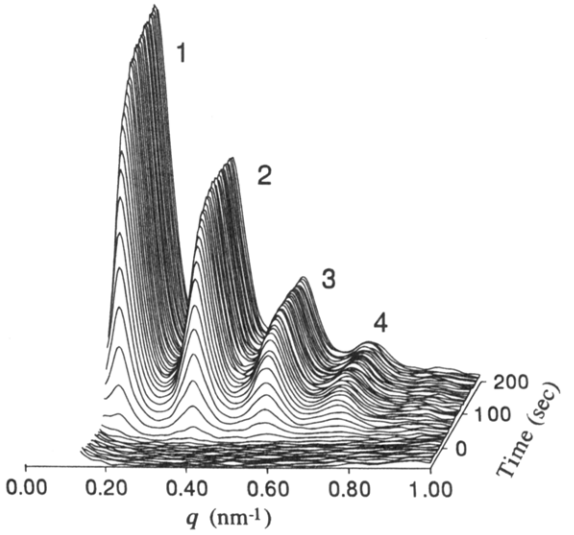

Figure 2. SAXS data for isothermal crystallization of E/EP 11/8 at 98 °C. Each data set is the q^2-corrected intensity integrated over 6 s. Time = 0 corresponds to the time at which the DSC thermocouple first registers T_c (98 °C). Numbers 1–4 indicate the reflection order from an alternating lamellar microstructure.

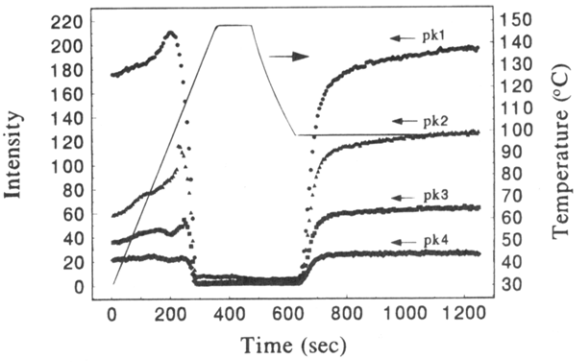

Figure 3. Peak intensity vs time for all four SAXS reflections for sample E/EP 11/8. Final peak positions are as follows: (●) $q_1 = 0.184$ nm^{-1}, (▲) $q_2 = 0.367$ nm^{-1}, (■) $q_3 = 0.547$ nm^{-1}, (◆) $q_4 = 0.726$ nm^{-1}. Time = 0 is the time at which the DSC thermocouple first registers T_c. The solid line represents the temperature which is referenced to the right axis.

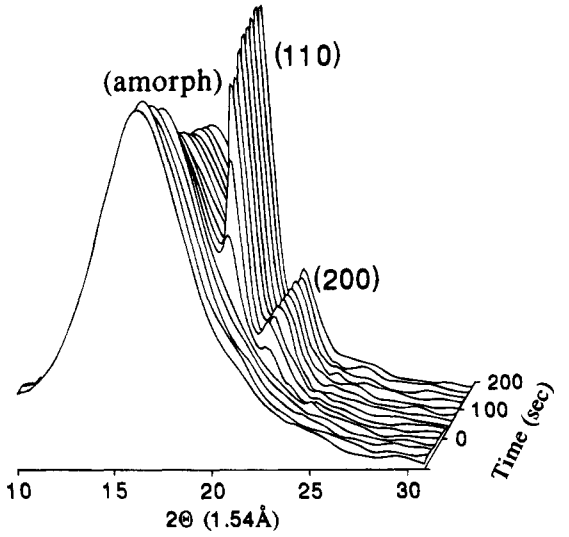

Figure 4. WAXS data for sample E/EP 11/8, corresponding to the SAXS data in Figure 2. Averaging of three consecutive patterns was done to improve clarity. Peaks labeled (110) and (200) are the reflections of the orthorhombic polyethylene unit cell; (amorph) represents the scattering from the EP and amorphous E.

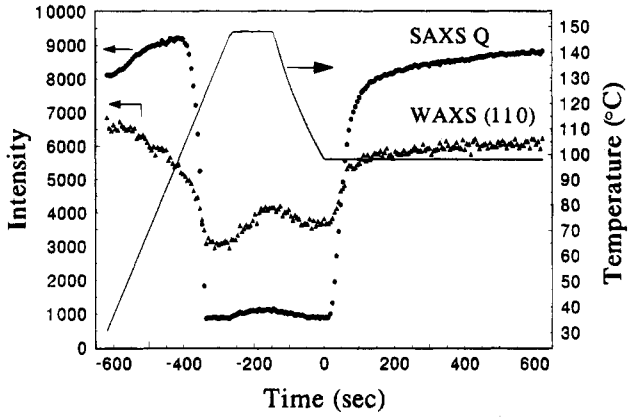

Figure 5. SAXS invariant Q (●) and WAXS (110) peak intensity (▲) vs time for sample E/EP 11/8. The solid line is the temperature which is referenced to the right axis. No background subtraction has been employed here for either SAXS or WAXS; the two data sets thus have nonzero values in the melt ($-350 < t < 30$ s).

to the SAXS data in Figure 2; for clarity each WAXS profile shown is the average of three consecutive frames (18 s). Unlike the SAXS data, WAXS melt scattering is not featureless but shows a large amorphous hump which decreases in intensity as the crystallite peaks begin to grow. The two crystallite peaks are the (110) and (200) peaks of the orthorhombic PE crystal.[12,23] The area under the crystalline peaks (I_c) and the amorphous scattering (I_a) can be used to estimate the weight fraction crystallinity within the E block, w_c:

$$w_c = \frac{1}{f}\left(\frac{I_c}{I_c + I_a}\right) \tag{1}$$

Values for the initial and final w_c are listed in Tables 1 and 2, respectively.

Figure 5 is a plot of the time evolution of the WAXS (110) peak intensity and the SAXS invariant Q. The SAXS invariant represents the electron density contrast in the sample, independent of the type of morphological features, and is properly obtained from the following integral:

$$Q = \int_0^\infty I(q)\, q^2 dq \tag{2}$$

The true invariant requires absolute intensity measurements, subtraction of the thermal density fluctuation background, and extrapolation to $q = 0$ and ∞; here, we employ a relative invariant, which is simply the total area of the q^2-corrected SAXS profile. The parallel growth of Q with crystalline peak intensity confirms that crystallization is the driving force for microphase separation.

The initial stage of isothermal development (at $T = T_c$) occurs from approximately $0 < t < 2t_{1/2}$, where $t_{1/2}$ is the crystallization half-time, the time when the intensity reaches half its final value. Values of $t_{1/2}$ for all polymers are listed in Table 2. This initial stage is characterized by a rapid increase in SAXS and WAXS intensities and is referred to as the "primary" process. Figure 6 is a plot of the SAXS peak position (q^*), peak width (Δq), and the SAXS Q versus time for the primary peak of sample E/EP 11/8; the vertical dashed line in Figure 6 corresponds to $2t_{1/2}$ for this sample. Before determining q^* and Δq, an approximate correction for the diffuse background scattering was made by subtracting the melt SAXS pattern at t_0. Peak widths (Δq) are determined as the full width at 85% of maximum intensity. During the primary growth phase of E/EP 11/8, q^* remains constant to within experimental error, while Δq appears to decrease by about 6%. For most of the diblocks, q^* and Δq show no discernable trend during this primary growth process, indicating that q^* is constant to better than 1% and Δq changes by no more than 5%. This contrasts with the 20% increase in q^* and 25% decrease in Δq observed for $0 < t < 2t_{1/2}$ for the hydrogenated polybutadiene sample E 52 (Figure 7).

At about $2t_{1/2}$, q^* for sample E 52 assumes a constant value, although the SAXS and WAXS intensities continue to increase slowly. In contrast, all the diblocks show a definite increase in q^* (Figure 6) accompanying the growth in intensity during this secondary stage ($t > 2t_{1/2}$). For the diblocks, the main peak at q^* represents the overall lamellar repeat distance d, as shown in Figure 1:

$$d = 2\pi/q^* \tag{3}$$

As discussed in the Introduction, the SAXS peak for sample E 52 represents the sum of the crystallite and amorphous layer widths, and applying eq 3 yields d' in place of d. Table 2 lists the relative increase in the SAXS invariant (ΔQ) and decrease in d ($-\Delta d$) between $2t_{1/2}$ and the end of each experiment (600 s after t_0).

IV. Discussion

To understand the ordering process in these semicrystalline diblocks, it is useful to compare it with the relevant processes in semicrystalline homopolymers (crystallization) and amorphous block copolymers (microphase separation). The multiple reflections present in the SAXS patterns indicate that our semicrystalline diblocks form a well-ordered microdomain structure with rather sharp domain interfaces even for small undercoolings. When these block copolymers crystallize from a single-phase melt, the E block expels the amorphous chains during crystallization; thus the density differential and sharp interface are established as soon as the E block crystallizes, as with homopolymer crystallization. As is usual for polymer crystallization,

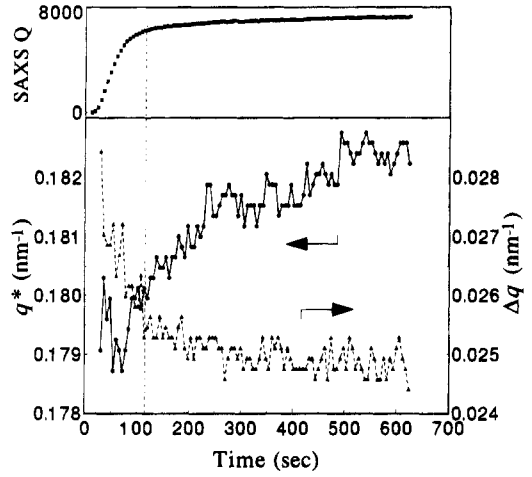

Figure 6. Peak position (●, left axis), peak width (▲, right axis) and background-subtracted SAXS invariant (■, top) vs time for sample E/EP 11/8. The dashed line represents $t = 2t_{1/2}$ (116 s) for this sample.

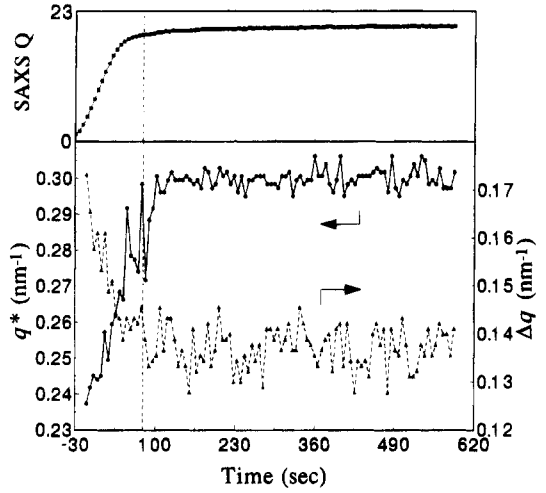

Figure 7. Peak position (●, left axis), peak width (▲, right axis) and background-subtracted SAXS invariant (■, top) vs time for sample E 52. The dashed line represents the maximum possible value of $2t_{1/2}$ (80 s) for this sample.

the rate of structure formation is a strong function of the undercooling. For symmetric amorphous block copolymers, the weakly-segregated structures which form at small undercoolings have broad domain interfaces and an essentially sinusoidal composition profile, yielding only a single SAXS reflection.[1,3] Deeper quenches will result in increased segregation strength and the appearance of higher-order reflections. In this case, if the mechanism of microphase separation resembles spinodal decomposition,[10,11] the higher-order peaks should appear sequentially as the domain interfaces sharpen, rather than growing at the same rate as the primary reflection. So far, no time-resolved data are available to comment on this case, due to the difficulty of achieving a large and rapid temperature drop which is uniform throughout the sample.

We have previously shown that our E/EP diblocks form spherulites when crystallized from the quiescent melt,[12] and time-resolved small-angle light scattering on sample E/EP 19/30 also shows the progressive growth of spherulites during isothermal crystallization.[30] The morphology depicted in Figure 1 was inferred, in part, from these observations.[12] Since the melt is homogeneous, there is no preexisting structure to confine the growing crystallites. Microphase separation develops only as a result of crystallization. In the contrasting case of a strongly-segregated lamellar material, crystallites may be restricted to grow only in the planes of the lamellae. Additionally, Douzinas and Cohen[22] have shown that the crystallites orient perpendicular to the lamellar surface in such materials, rather than parallel as shown in Figure 1. These morphological differences may be reflected in the crystallization kinetics as well, an area for future research. Our observations on a diblock crystallizing from a weakly-segregated melt will be reported separately.[31]

Initial Growth Stage. The primary stage of crystallization in our diblocks, corresponding roughly to $0 < t < 2t_{1/2}$, is characterized by little change in d (see q^* in Figure 6) and parallel growth of multiple SAXS peaks (Figure 3). This suggests that, on crystallization, spherulites grow to fill the sample volume with little accompanying change in their internal microstructure. This growth mechanism also suggests that the WAXS and SAXS data should evolve identically with time, since the only change which occurs is the progressive crystallization of homogeneous melt into radially growing lamellae. To test whether the various SAXS and WAXS peaks truly develop in parallel, it is useful to replot the data in the Avrami form, which is commonly used to analyze crystallization processes:

$$\ln(1 - X_c) = -kt^n \tag{4}$$

In polymer crystallization, X_c is considered to be the fraction of sample that is filled with spherulites, t is the time elapsed, and k and n are system parameters. For the SAXS and WAXS data we obtain X_c from:

$$X_c = \frac{I(t) - I_0}{I_m - I_0} \tag{5}$$

where I_0 is the melt scattering intensity at T_c (determined from data sets immediately after t_0), I_m is the intensity at the end of the experiment, and $I(t)$ represents the intensity at time t. Because these polyethylene-based polymers crystallize rapidly, it is difficult to obtain truly isothermal crystallization. The actual cooling rate (20 °C/min) is not fast enough in all cases for the sample to remain fully amorphous until T_c is reached; in fact, sample E 52 shows growth in SAXS and WAXS intensity about 30 s before t_0. Also, after rapid cooling from the melt, the center of the sample cell remains above T_c until the temperature is equalized through conduction. The detailed shape of the Avrami plot (log–log representation of eq 4), as well as the best-fit value of n, can be strongly influenced by these factors. However, we employ the Avrami form here merely to show that the SAXS and WAXS intensities track each other while the structure forms; if the two truly develop in parallel, then their Avrami plots will superimpose even if crystallization is not isothermal.

The scaled intensities of the WAXS (110) reflection and all four SAXS peaks for sample E/EP 11/8 superimpose quite well on the Avrami plot in Figure 8. The X_c functions calculated from the SAXS and WAXS data have a somewhat different significance since the SAXS data reflect the fraction of the sample which is microphase separated, while the WAXS data reflect the fraction which has crystallized. Thus the superposition of the SAXS and WAXS data sets on the Avrami plot indicates that the ordering process closely follows the crystallization kinetics, for all X_c between 0.01 and 1.

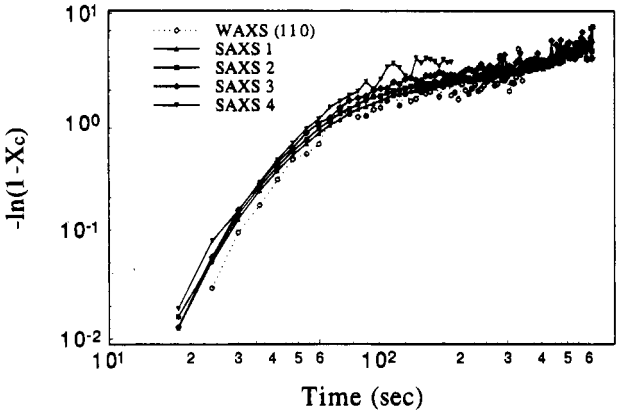

Figure 8. Avrami plot of the four SAXS peaks and the (110) WAXS reflection for sample E/EP 11/8.

Also, the simultaneous growth of all SAXS peak orders is emphasized.

By comparison, sample E 52 shows considerable structural reorganization during the initial growth stage ($0 < t < 2t_{1/2}$; see Figure 7). During this period, the intercrystallite repeat distance d' decreases by 20%, and the peak width also decreases by about 25%, suggesting that primary and secondary crystallization processes overlap in E 52 for this choice of undercooling.[17] Since d' decreases with time, this change is clearly not the result of lamellar thickening, which occurs when chain folding is caused by kinetic limitations; in these random ethylene–butene systems, the crystallite size is limited by the ethyl branch frequency, not kinetics. Prior work on crystalline homopolymers[15,17] has elucidated two other secondary crystallization mechanisms: creation of new lamellar stacks (d' is constant) and creation of new lamellae from the amorphous material between the existing lamellae (d' decreases). The latter mechanism is consistent with the reductions in d' and peak width, as observed.

Later Growth Stage. Beyond $2t_{1/2}$, the SAXS and WAXS intensities for sample E 52 continue to increase in parallel, though at a greatly reduced rate, but this is not accompanied by any perceptible change in d'. The diblocks also show two distinct stages of SAXS and WAXS intensity growth. As in sample E 52, the diblock SAXS and WAXS intensities continue to increase slowly and in parallel for $t > 2t_{1/2}$ (Figures 5 and 8), but all of the diblocks also show a decrease in d during this stage (see q^* in Figure 6). A possibility qualitatively consistent with the trends in the diblock data would be the formation of additional interlamellar crystallites within the E domain. Recall that, for the block copolymers, the repeat distance probed by SAXS is d, not d'. If the crystallites already present within the E domain prevent rearrangement of the microphase-separated morphology, then the EP domain width should remain constant during the additional crystallization, while d will decrease slightly as the E domain thins due to an increase in its density. Using the known mass densities of amorphous and crystalline E, EE, and EP,[21,23,32] the electron density difference $\Delta\rho$ between the E and EP domains can be calculated as a function of w_c. Therefore, the observed ΔQ can be used to estimate the change in w_c and hence the change in d which would result from interlamellar secondary crystallization. This calculation can reproduce at most 17% of the observed Δd; moreover, note that the values of ΔQ and Δd (Table 2) are apparently uncorrelated. Zachmann and Wutz[15] have suggested that, when SAXS and WAXS intensities increase at the same rate, it is due to a secondary crystallization process in which new lamellar stacks are created; in our case this corresponds to the conversion of additional homogeneous melt to microphase separated material. This explanation is consistent with the block copolymer data as well as the 2.3% increase in Q observed for E 52 with no concomitant change in d'. On the SAXS and WAXS length scales, then, this type of secondary crystallization differs from the initial crystallization only in its rate.

The decrease in d for the diblocks for $t > 2t_{1/2}$ would thus reflect a contraction of the E and EP (or EE) domains within the already-formed structure. A possible driving force for this rearrangement is that it allows the amorphous block to adopt a less-stretched conformation. The two theories that describe crystallization-driven morphology model the chains in the two blocks as a compromise between the random-coil configuration preferred by the amorphous chains and the extended-chain conformation of the crystallites.[13,14] Since the kinetics of E crystallization are very fast (half times from 0.5 to 2 min), it is possible that the initial morphology is a nonequilibrium one favoring the crystallites. Over time this structure could equilibrate to give a morphology in which the amorphous chains are more relaxed, thus lowering d.

V. Conclusions

Time-resolved simultaneous SAXS, WAXS, and DSC were performed on E/EP and E/EE semicrystalline diblock copolymers to study microphase separation and its relationship to crystallization. During isothermal crystallization the first- and higher-order SAXS peaks appear concurrently and grow at the same pace, indicating that the density differential and sharp interface are established as soon as the E block crystallizes. During the primary stage ($0 < t < 2t_{1/2}$) of crystallization, the diblock SAXS patterns exhibit constant peak positions, indicating that growth of the ordered structure occurs with little or no internal rearrangement of the domains. This contrasts with a hydrogenated polybutadiene sample (E 52), which shows substantial changes in the crystallite size distribution over the same period. The superposition of SAXS and WAXS data for the diblocks on an Avrami plot indicates that microstructure and crystallinity follow identical growth kinetics.

For $t > 2t_{1/2}$ the SAXS and WAXS intensities for the diblocks continue to grow in parallel, but at a much-reduced rate; simultaneously, d decreases slightly. Calculations indicate that the observed decrease in d cannot be explained quantitatively by the formation of interlamellar crystallites within the E domain. We attribute the parallel growth of the SAXS and WAXS intensities in this later stage to the creation of new lamellar stacks—new regions of microphase-separated material that were previously homogeneous melt. The slight decrease in d for the diblocks, which must reflect a contraction of both the crystalline and amorphous domains, is attributed to relaxation of the amorphous chains from an original nonequilibrium extended conformation frozen-in during crystallization. Thus, these semicrystalline diblocks exhibit features reminiscent of crystallization in homopolymers, as well as microphase separation in amorphous block copolymers. As in homopolymer crystallization, a domain structure with sharp interfaces is formed even for small undercoolings. As with microphase separation in amorphous block

copolymers, the period of the ordered structure is essentially invariant during the crystallization process and is fixed by the molecular architecture of the chain.

Acknowledgment. Support for this research (to P.R. and R.A.R.) was provided through the National Science Foundation, Polymers Program (DMR-9257565), and the NEC Preceptorship at Princeton University.

References and Notes

(1) Floudas, G.; Pakula, T.; Fischer, E. W.; Hadjichristidis, N.; Pispas, S. *Acta Polym.* **1994**, *45*, 176.
(2) Rosedale, J. H.; Bates, F. S. *Macromolecules* **1990**, *23*, 2329.
(3) Schuler, M.; Stühn, B. *Macromolecules* **1993**, *26*, 112.
(4) Harkless, C. R.; Singh, M. A.; Nagler, S. E.; Stephenson, G. B.; Jordan-Sweet, J. L. *Phys. Rev. Lett.* **1990**, *64*, 2285.
(5) Leibler, L. *Macromolecules* **1980**, *13*, 1602.
(6) Frederickson, G. H.; Helfand, E. *J. Chem. Phys.* **1987**, *87*, 697.
(7) Bates, F. S.; Bair, H. E.; Hartney, M. A. *Macromolecules* **1984**, *17*, 1987.
(8) Helfand, E.; Wasserman, Z. R. In *Developments in Block Copolymers-1*; Goodman, I., Ed.; Applied Science: New York, 1982.
(9) Molau, G. E. In *Block Copolymers*; Aggarwal, S. L., Ed.; Plenum: New York, 1970.
(10) Hashimoto, T. *Macromolecules* **1987**, *20*, 465.
(11) Fredrickson, G. H.; Binder, K. *J. Chem. Phys.* **1989**, *91*, 7265.
(12) Rangarajan, P.; Register, R. A.; Fetters, L. J. *Macromolecules* **1993**, *26*, 4640.
(13) DiMarzio, E. A.; Guttman, C. M.; Hoffman, J. D. *Macromolecules* **1980**, *13*, 1194.
(14) Whitmore, M. D.; Noolandi, J. *Macromolecules* **1988**, *21*, 1482.
(15) Zachmann, H. G.; Wutz, C. *Polym. Prepr. (Am. Chem. Soc., Div. Polym. Chem.)* **1992**, *33*, 261.
(16) Song, H. H.; Stein, R. S.; Wu, D.-Q.; Ree, M.; Phillips, J. C.; LeGrand, A.; Chu, B. *Macromolecules* **1988**, *21*, 1180.
(17) Schultz, J. M. *Makromol. Chem., Macromol. Symp.* **1988**, *15*, 339.
(18) Ryan, A. J.; Komanschek, B. U.; Naylor, S.; Bras, W.; Mant, G. R.; Derbyshire, G. E. In *Hyphenated Techniques in Polymer Characterization*: Provder, T. Ed.; ACS Symposium Series; American Chemical Society: Washington, DC, 1994; in press.
(19) Cohen, R. E.; Cheng, P. L.; Douzinas, K.; Kofinas, P.; Berney, C. V. *Macromolecules* **1990**, *23*, 324.
(20) Séguéla, R.; Prud'homme, J. *Polymer* **1989**, *30*, 1446.
(21) Bates, F. S.; Schulz, M. F.; Rosedale, J. H.; Almdal, K. *Macromolecules* **1992**, *25*, 5547.
(22) Douzinas, K. C.; Cohen, R. E. *Macromolecules* **1992**, *25*, 5030.
(23) Howard, P. R.; Crist, B. *J. Polym. Sci. Part B: Polym. Phys.* **1989**, *27*, 2269.
(24) Morton, M.; Fetters, L. J. *Rubber Chem. Technol.* **1975**, *48*, 359.
(25) Rosedale, J. H.; Bates, F. S. *J. Am. Chem. Soc.* **1988**, *110*, 3542.
(26) Hadjichristidis, N.; Xu, Z.; Fetters, L. J.; Roovers, J. *J. Polym. Sci., Polym. Phys. Ed.* **1982**, *20*, 743.
(27) Bras, W.; Derbyshire, G. E.; Ryan, A. J.; Mant, G. R.; Felton, A.; Lewis, R. A.; Hall, C. J.; Greaves, G. N. *Nucl. Instrum. Methods Phys. Res., Sect. A* **1993**, *326*, 587.
(28) Bras, W.; Derbyshire, G. E.; Cooke, J.; Komanschek, B. E.; Devine, A.; Clark, S. M.; Ryan, A. J. *J. Appl. Cryst.*, accepted for publication.
(29) Russell, T. P. in *Handbook on Synchrotron Radiation*; Brown, G. S., Moncton, D. E., Eds.; North-Holland: New York, 1991; Vol. 3.
(30) Ueda, M.; Rangarajan, P.; Register, R. A., unpublished results.
(31) Rangarajan, P.; Register, R. A.; Fetters, L. J.; Bras, W.; Naylor, S.; Ryan, A. J. *Macromolecules*, to be submitted.
(32) Krishnamoorti, R. Ph.D. Thesis, Princeton University, Princeton, NJ, 1993.

MA941278C